A fluorescence resonance energy transfer-derived structure of a quantum dot-protein bioconjugate nanoassembly

I. L. Medintz*[†‡], J. H. Konnert[†§], A. R. Clapp[¶], I. Stanish*, M. E. Twigg[‖], H. Mattoussi[¶**], J. M. Mauro*[,††], and J. R. Deschamps[§]

*Center for Bio/Molecular Science and Engineering, Code 6900, [§]Laboratory for the Structure of Matter, Code 6030, [¶]Division of Optical Sciences, Code 5611, and [‖]Electronics Science and Technology Division, Code 6812, U.S. Naval Research Laboratory, Washington, DC 20375

Communicated by Jerome Karle, Naval Research Laboratory, Washington, DC, May 12, 2004 (received for review February 23, 2004)

The first generation of luminescent semiconductor quantum dot (QD)-based hybrid inorganic biomaterials and sensors is now being developed. It is crucial to understand how bioreceptors, especially proteins, interact with these inorganic nanomaterials. As a model system for study, we use Rhodamine red-labeled engineered variants of *Escherichia coli* maltose-binding protein (MBP) coordinated to the surface of 555-nm emitting CdSe-ZnS core–shell QDs. Fluorescence resonance energy transfer studies were performed to determine the distance from each of six unique MBP-Rhodamine red dye-acceptor locations to the center of the energy-donating QD. In a strategy analogous to a nanoscale global positioning system determination, we use the intraassembly distances determined from the fluorescence resonance energy transfer measurements, the MBP crystallographic coordinates, and a least-squares approach to determine the orientation of the MBP relative to the QD surface. Results indicate that MBP has a preferred orientation on the QD surface. The refined model is in agreement with other evidence, which indicates coordination of the protein to the QD occurs by means of its C-terminal pentahistidine tail, and the size of the QD estimated from the model is in good agreement with physical measurements of QD size. The approach detailed here may be useful in determining the orientation of proteins in other hybrid protein–nanoparticle materials. To our knowledge, this is the first structural model of a hybrid luminescent QD-protein receptor assembly elucidated by using spectroscopic measurements in conjunction with crystallographic and other data.

maltose-binding protein | three-dimensional structure | nanotechnology | nanocrystal

The burgeoning field of nanotechnology promises to revolutionize many scientific fields, and the first generation of functional hybrid nanomaterials exploring the interface between biology and materials science is now being developed and prototyped (1–3). One exciting avenue of biomaterials research involves protein–nanomaterial composites (2–4). Proteins lend many of their unique properties to these hybrid materials, such as: assisting in ordered self-assembly processes such as that of Pd nanoparticles assembled on tubulin or viral assembly of orientated nanowires (5, 6), engendering exquisite biorecognition properties such as the receptors used in hybrid nanocrystal biosensors (7), and catalyzing useful electrochemical and cleavage reactions (2, 8). Of critical importance in developing these materials is a fundamental understanding of how proteins or bioreceptors interact with inorganic nanomaterials.

The unique properties of luminescent colloidal semiconductor nanocrystals or quantum dots (QDs) have recently been incorporated into hybrid functional nanoassemblies. Cadmium selenide-zinc sulfide (CdSe-ZnS) core–shell QDs, in particular, have exceptional photochemical stability and relatively high quantum yields, as well as broad excitation and size-tunable photoluminescence spectra with narrow emission bandwidths (full width at half maximum of ≈25–45 nm) that span the visible spectrum, allowing simultaneous excitation of several particle sizes at a single wavelength (9). To date, most biological applications have focused on using QDs in a semipassive role as protein- or DNA-conjugated fluorometric labels for cellular imaging, in immunoassays, or entrapped in polymer beads for optical bar coding (9–15).

To create QD bioconjugates for various assays, and to study ordered assembly processes, a variety of proteins have been either covalently attached or electrostatically self-assembled onto QD surfaces (5, 6, 10, 14–22). Recently, QDs have assumed more active roles in a fluorescence resonance energy transfer (FRET) DNA replication monitoring system and as scaffolds and FRET donor molecules in prototype *in vitro* biosensors (7, 23, 24). The solution phase QD-FRET biosensors consisted of *Escherichia coli* maltose-binding proteins (MBPs) specifically attached to the ZnS surface of QDs by means of histidine metal affinity coordination (7). The central binding pocket of each QD-coordinated MBP was preloaded with a dye-labeled sugar analog, resulting in FRET quenching of the QD photoluminescence. Addition of the maltose target analyte to the QD-sensor solution displaced the dye-labeled analog altering FRET in a concentration-dependent manner (7). This same QD-MBP system was used for an in-depth study of FRET interactions between several QD donors with differing emission wavelengths and a dye-labeled MBP acceptor (24). In a further study, MBP labeled with the photochromic dye 1′,3-dihydro-1′-(2-carboxyethyl)-3,3-dimethyl-6-nitrospiro-[2H-1-benzopyran-2,2′-(2H)-indoline] (BIPS) was coordinated to the QD surface and the MBP-BIPS was used as a reversible photochromic modulator of QD photoluminescence (25). Although MBP is clearly functional in each of these solution phase nanoassemblies, the exact nature of the MBP-QD interaction(s) remain unknown.

Few high-resolution analytical techniques are available that can elucidate the nature of the solution phase QD–MBP interaction/orientation without introducing experimental artifacts. Preparatory steps for high-resolution transmission electron microscopy involve fixing proteins and metallic overcoating for contrast, which may denature the protein. The physical properties of QDs themselves interfere with spectroscopic techniques such as NMR and circular dichroism. However, FRET studies

Abbreviations: RR, Rhodamine red; MBP, maltose-binding protein; QD, quantum dot; FRET, fluorescence resonance energy transfer; D/P, dye/protein ratio; MSD, mean square distance deviation.

[†]I.L.M. and J.H.K. contributed equally to this work.

[‡]To whom correspondence may be addressed at: Center for Bio/Molecular Science and Engineering, Code 6910, U.S. Naval Research Laboratory, 4555 Overlook Avenue SW, Washington, DC 20375. E-mail: imedintz@cbmse.nrl.navy.mil.

**To whom correspondence may be addressed at: Division of Optical Sciences, Code 5611, U.S. Naval Research Laboratory, 4555 Overlook Avenue SW, Washington, DC 20375. E-mail: hedimat@ccs.nrl.navy.mil.

[††]Present address: Molecular Probes, Inc., 29851 Willow Creek Road, Eugene, OR 97402.

www.pnas.org/cgi/doi/10.1073/pnas.0403343101

have been used extensively to determine numerous protein–protein interactions (26–37). These studies include positioning troponin residues on the actin filament (28), determining the global structure of the VS ribozyme (29), mapping the antagonist-binding site of serotonin type 3 receptor (30), determining the structural organization of the synaptic exocytosis core (31), and defining the orientation of MRE-binding transcription factor 1 (32), as well as analyzing the spatial relationships between proteins of the nuclear pore complex (33). Some research groups have gone further by using FRET results along with other available data, including crystallographic coordinates, to create integrated models of troponin-1 in complex with troponin-C, clustering of CD8 with TCR, and folding of phosphoglycerate kinase (34–37).

We describe here a FRET-based modeling technique for determining the solution phase orientation of a protein, MBP, as coordinated to the QD surface. Six different single-cysteine MBP mutants, spatially distributed on the protein surface, were specifically labeled with Rhodamine red (RR) dye and individual QD-RR-labeled MBP protein assemblies were prepared. The distance from each of the six different RR-acceptor MBP locations to the center of the energy-donating QD was derived from FRET efficiency data. The orientation of the bound MBP with respect to the QD surface was modeled and refined from the donor-acceptor distances in conjunction with the crystallographic coordinates of MBP by using a method analogous to a nanoscale global positioning system determination. The MBP orientation and QD-MBP model are in agreement with other physical data gathered. The orientation of the protein with respect to the QD surface is an important feature of the assembly with a direct link to the biological properties of the assembly. Information from such a model can be used to enhance desirable properties in future constructs. The derived orientation can be further exploited through homology modeling to produce entirely new constructs from closely related proteins.

Materials and Methods

MBP. MBP (M_r ≈44 kDa) encoded on a plasmid vector was purified as described (17, 38). By using standard recombinant techniques, the MBP sequence was engineered to express a C-terminal five-histidine sequence along with individual mutants having Asp-41, Thr-80, Asp-95, Ala-34, Ala-215, or Ala-292 changed to cysteine (MBP41C, MBP80C, MBP95C, MBP134C, MBP215C, and MBP292C; refs. 38 and 39). The locations of these mutations were selected to produce substitution in both lobes of MBP (Fig. 1*A*). Nomenclature refers to the original sequence (40); see Table 3, which is published as supporting information on the PNAS web site, for the current sequence. Sequence-verified MBP mutants were expressed in *E. coli* TOP10 cells (Stratagene) and purified (41). Individual MBP mutants were labeled with monofunctional RR (Fig. 1*B*) maleimide (Molecular Probes) after disulfide reduction with DTT as described (41). All proteins were labeled with a dye/protein ratio (D/P) of ≈1, except MBP215C, which had a D/P of ≈0.4. Prior attempts to label this MBP mutant with other dyes also resulted in a low D/P, suggesting issues of dye accessibility (data not shown).

QD Synthesis and MBP-Bioconjugate Assembly. The 555-nm emitting CdSe-ZnS core–shell QDs were prepared as described (42). QDs were rendered water soluble by replacing the native TOP/TOPO organic capping shell with bidentate dihydrolipoic acid (dithiol-alkyl-COOH) ligands (17). For bioconjugate assembly, see *Supporting Materials and Methods*, which is published as supporting information on the PNAS web site.

QD MBP-Bioconjugate Modeling. The crystallographic structure/coordinates of MBP, PDB ID code 1LLS (which can be accessed at www.rcsb.org/pdb; ref. 43) were used. All coordinates reported are expressed in the 1LLS system. By using the program MIDAS (44), the six indicated MBP residues in the x-ray structure were modified to cysteine. RR structures were attached at the sulfur atoms (Fig. 1*A*) and MBP-RR torsion angles were manipulated for each to estimate average dye-acceptor center distances from the cysteine sulfur atoms (Figs. 1 and 3 *A* and *B*). We assume that the dye-acceptor positions are constrained to be >8 Å but <12 Å from the cysteine sulfurs and >6 Å from any other protein atom; see Figs. 3 *A* and 1*B*. The 18 parameters defining the MBP dye-acceptor positions plus three coordinates for the QD center define the 21 parameters to be estimated. We sample the volume around each cysteine sulfur atom within which the acceptor is constrained with a cubic closely packed array of points. Each sample point represents 8 Å^3. The number of volume elements associated with each acceptor is given in the right column of Table 1. The number of combinations of these elements, taking one element for each acceptor, is 3.32×10^{11} (product of the number of allowed volume elements for each acceptor). The number of combinations increases inversely with the sixth power of the volume element size. For each of these combinations, we carry out a least-squares procedure that minimizes the mean square distance deviation (MSD) for the distances between the experimentally measured distances, d_{ex}, and the computed distances, d_o. Each refinement varies only the

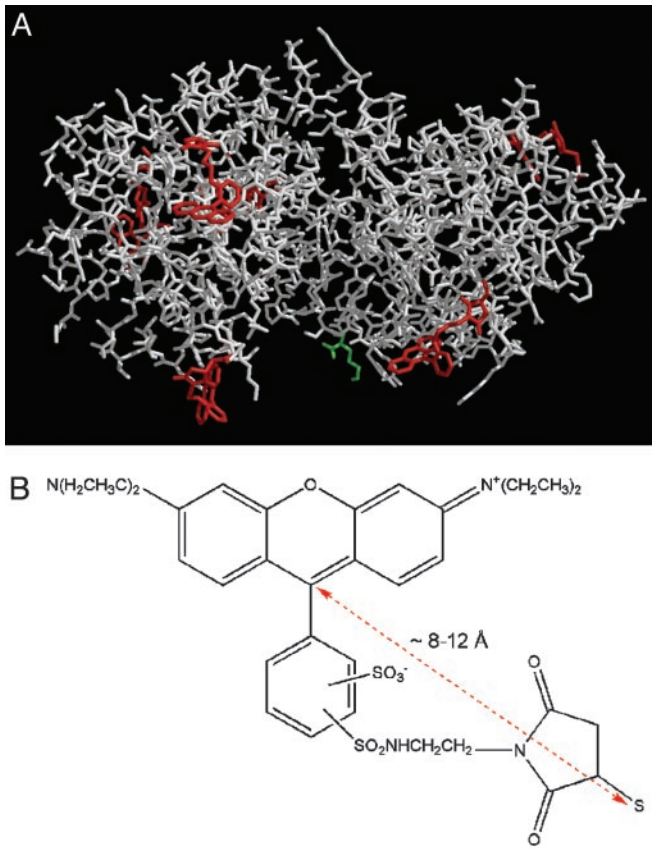

Fig. 1. MBP crystal structure highlighting location of residues labeled with RR. (*A*) MBP (gray) with RR maleimide structures attached at 41C, 80C, 95C, 134C, 215C, and 292C in red. The terminal Lys-370 side chain in the PDB ID code 1LLS structure is green. This residue is the point of attachment for a glycine-serine linker and a terminal pentahistidine sequence in the MBP used. (*B*) Chemical structure of maleimide-active RR shown conjugated to a representative sulfur atom S from a cysteine residue. The minimum/maximum torsion distances from this sulfur atom to the central carbon of the dye structure are ≈8–12 Å.

BIOPHYSICS

Table 1. Measured and calculated data values

MBP mutant	Measured distance (r) determined from corrected FRET titration data	Refined distance	Δ	No. of positions considered for 8–12 Å shells
41C	72.9 ± 2.2	72.9	+0.0	185
80C	58.9 ± 0.7	63.0	−4.1	116
95C	87.5 ± 3.3	79.0	+8.5	31
134C	75.1 ± 3.7	81.3	−6.2	141
215C	94.5 ± 2.0	91.7	+2.8	118
292C	90.4 ± 2.9	91.1	−0.7	30

three parameters for the QD position. The distribution of the estimates for the QD position as a function of the MSD associated with each refinement yields a qualitative estimate for the accuracy in determining the QD position. A least-squares refinement may be expressed as the minimization of F in Eq. **1** (45).

$$F = \sum_{i=1,N} \frac{1}{\sigma_i^2}[d_{i,ex} - d_{i,o}]^2 = \sum w^2\Delta^2 \qquad [1]$$

Although each FRET measurement has an SD, σ, associated with it, we used equal weights, w, in Eq. **1** because of the uncertainty in the acceptor center positions. Thus, the function minimized was the MSD.

$$\text{MSD} = \frac{1}{6}\sum_{i=1,6}[d_{i,ex} - d_{i,o}]^2 \qquad [2]$$

Supporting Materials and Methods. QD-MBP-RR bioconjugate FRET titrations and data analysis, atomic force microscopy, transmission electron microscopy, and QD size determination can be found in *Supporting Materials and Methods*.

Results

FRET-Derived MBP Mutant-QD Center Distances. Each of the six MBP mutants, three located in each of the two MBP globular domains (Fig. 1*A*), was labeled with RR as described at a D/P of 1, except for MBP215C. A series of QD-MBP-RR FRET titrations was performed where MBP-RR to QD ratios were varied among samples from 0 to 10, whereas the overall amount of MBP coordinated to QD was maintained at 15 (see Fig. 2). Data for MBP215C was adjusted accordingly. A titration series allows for a more accurate estimate of overall FRET efficiency than does a single measurement (24). Direct excitation-corrected RR-acceptor enhancement was used to measure FRET efficiency and derive the distance from each RR dye location to the QD center (see Table 1). Because the FRET efficiency data are essentially a measurement of distance from QD center to the dye, the use of different dyes, with different linker lengths and concomitant differing physical properties (hydrophobic versus hydrophilic interactions with the protein) will derive a different distance value (24). Therefore, it is important to use the same dye for a particular structural elucidation.

Modeling of QD-Coordinated MBP Orientation. The objective was to determine the position and orientation of the MBP with respect to the QD center by using the distance values (r) obtained with FRET measurements. This situation would be a straightforward least-squares problem if the positions of the RR acceptor centers were known. However, we know only that the acceptors are attached to the cysteine sulfurs of the point mutation sites with constraints on the volumes they may occupy based on RR acceptor size, the length of the linker, and the surrounding

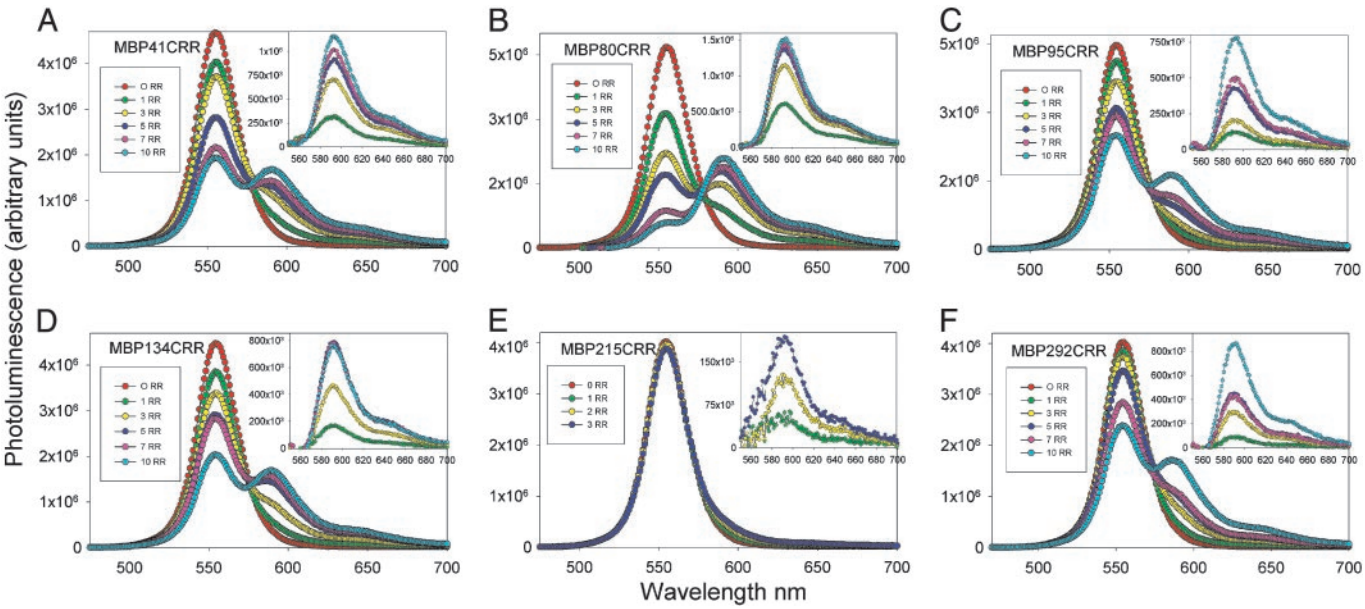

Fig. 2. FRET titration data for 555-nm QDs and an increasing ratio of MBP41C-RR (*A*), MBP80C-RR (*B*), MBP95C-RR (*C*), MBP134C-RR (*D*), MBP215C-RR (*E*), and MBP292C-RR (*F*). Uncorrected FRET titration data are presented for each of the six MBP mutant-QD ensembles. (*Insets*) Shown are the direct excitation-corrected MBP-RR FRET-enhanced data for each point. All proteins have a D/P of 1, except for MBP215C, which has a D/P of ≈0.4, and this titration adjusts accordingly.

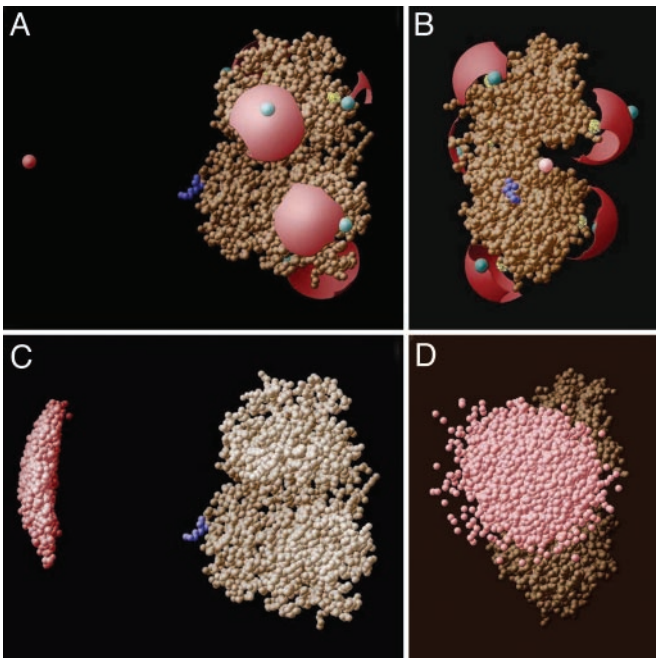

Fig. 3. Modeling of the allowed acceptor regions and QD center. (*A* and *B*) Side view (*A*) and 90°-shifted view (*B*) showing the structure of MBP with each of the six RR-conjugated cysteine mutant positions and the shells (pink) of radius 10 Å, indicating the allowed regions for the acceptors. The side chain of Lys-370 is blue. The red sphere is the QD center derived from the final refinement. The refined final dye-acceptor positions are teal and the yellow speckles show the cysteine sulfurs. (*C* and *D*) Side view (*C*) and 90°-shifted view (*D*) showing the positions of the estimated QD centers associated with the refinements having MSDs between the experimental and observed QD-acceptor distances <81 Å^2. All are in the same region of space. The minimum corresponding to the best estimate for the QD center has an MSD of 18 Å^2.

protein. The 18 parameters defining the six receptor positions plus three coordinates for the QD center define the parameters to be estimated. Although we may obtain estimates for the position of the QD center, the paucity of data present for estimating the values for this number of parameters makes the task of specifying precisely the accuracy of the resulting refinement difficult. One possible approach would be to set up a least-squares refinement of all 21 parameters with the constraints that the receptor positions not approach too near the MBP. This goal could be accomplished as an eigenvalue–eigenvector problem for which only the linear combinations of the 21 parameters best determined by the data are varied. We chose another approach, both for its simplicity, and because it maintains the separation of the QD variables from the dye-acceptor variables.

First, we sampled the volume around the cysteine sulfur of each MBP mutant within which the acceptor is constrained with a close packed cubic array of volume elements, each representing 8 Å^3. Manipulation of RR torsion angles in each of the six MBP mutants indicated that acceptor centers will most likely fall within a range of 8–12 Å from the cysteine sulfur atoms. We made the approximation that the dye-acceptor positions are constrained to be >8 Å but <12 Å from the cysteine sulfurs and >6 Å from any other protein atom. For each of these combinations of allowed volume elements, we carried out a least-squares procedure that minimizes the MSD between the experimentally measured distances and the computed distances and each refinement varies only the three parameters for the QD position. The distribution of the estimates for the QD position as a function of the MSD associated with each refinement yields a qualitative estimate for the accuracy in determining the QD position.

Table 2. Refined QD and MBP coordinates when MBP is oriented on the surface of a 555-nm QD (Cartesian coordinates relative to PDB ID code 1LLS)

MBP mutant	Refined acceptor position X	Refined acceptor position Y	Refined acceptor position Z
41C	−23.30	−20.70	−11.51
80C	17.76	−18.49	−16.55
95C	16.13	9.88	−3.93
134C	7.15	15.26	26.66
215C	−27.66	12.41	11.17
292C	−18.21	3.85	−21.21
QD center	21.59	−63.87	26.40

QD center to MBP residue 370 (shortest QD-to-MBP distance) ≈ 45 Å.

The minimum MSD obtained was 18 Å^2 or a root-mean-squares deviation of 4.2 Å. The QD center associated with this minimum is represented by the small red spheres in Fig. 3 *A* and *B*. NZ370 (blue) is the MBP atom on Lys-370 in the 1LLS structure. The associated probable positions for the locations of the dye acceptors are represented by the small teal spheres on the pink shells of radius 10 Å that illustrate, approximately, the allowed positions for the acceptors. The final refined coordinates for the QD center and MBP-acceptor positions are listed in Table 2. Fig. 3 *C* and *D* displays the volume containing all of the QD center position estimates for which the MSD was <81 Å^2. This volume includes the 10% of the 3.32×10^{11} refinement results with the lowest MSDs. All fall in the same region of space.

Whereas we cannot estimate accurately the error in the position for the QD center, we can look at the individual refinement associated with the lowest MSD. Because the QD center distribution versus MSD shown in Fig. 3 *C* and *D* indicates the smallest spread in the direction toward the MBP, we transform the coordinates to a system in which the x axis is parallel to the line through the QD center and the average position of the six cysteine sulfur atoms. The new z coordinate is perpendicular to the plane of Fig. 3*C*. The least-squares procedure yields coordinates for the QD center (x_o, y_o, z_o), with an associated SD of $\sigma(X_o) = 3.01$ Å, $\sigma(Y_o) = 11.25$ Å, $\sigma(Z_o) = 12.34$ Å; see Table 2. An ellipsoid with axis values of 1.54 times the σ values will enclose the volume within which there is a 50% probability of finding the QD center. This ellipsoid is nearly the same shape and size as the region illustrated in Fig. 3 *C* and *D*, within which fall the estimated QD centers associated with the smallest MSDs.

The refined QD center is nearest Lys-370 at a distance of ≈45 Å. Fig. 4*A* shows a stick model of MBP attached to a spheroid defining the QD space. Each of the six acceptor-dye centers are joined to the QD center by imaginary lines representing the FRET-derived r values. Fig. 4*B* shows a space-filling model of both the QD and the surface coordinated MBP. A further half-shell is presented to illustrate the position of the dihydrolipoic acid ligand.

Discussion and Conclusions

We have demonstrated that MBP appended with a C-terminal pentahistidine sequence coordinates to the surface of QDs by means of histidine-zinc metal affinity, yet retains almost unaltered analyte sensitivity and specificity (7). The strategy used here to elucidate the MBP structure as coordinated to the QD surface is essentially a nanoscale global positioning system determination (46). In a method analogous to triangulating a point on the globe from orbiting satellites, we start with the six dye-acceptor positions on the protein (our satellite locations and

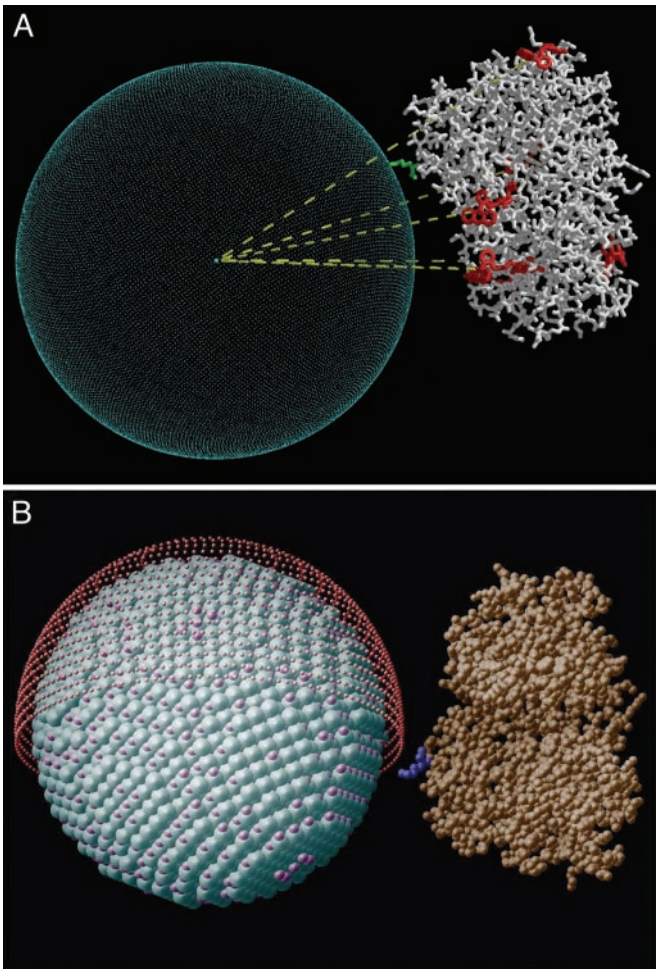

Fig. 4. Refined MBP QD orientation. (*A*) Side view presenting the structure of the final refined MBP orientation with all six RR structures positioned, in red. The refined distances from each of these RRs to the center of the spheroid are yellow. By using this refinement, ≈45 Å is estimated as the radius of the spheroid (or the distance from the nearest MBP atom of Lys-370, green, in the PDB ID code 1LLS structure to the QD center). (*B*) View of final refined orientation of MBP relative to the QD (space-filling) is presented with QD surface sulfur atoms in teal and zinc atoms in pink. The red shell shows the estimated outer radius of the dihydrolipoic acid ligand. Note that neither structure accounts for the pentahistidine sequence and the Gly-Ser linker attached to Lys-370.

the protein crystal structure fixes relative satellite positions) and locate the center of the QD (our globe with MBP satellites in orbit) by using FRET-derived *r* values (distances from each MBP satellite position to the center of the globe; Fig. 4*A*). In theory, this nanoscale global positioning system problem could be accomplished as a triangulation with as few as four noncoplanar locations.

Our procedure is similar to that used in determining the intramolecular distances of yeast phosphoglycerate kinase (YPK) domains during protein folding (36, 37), which used six FRET distance measurements between locations in two domains assumed to be rigid and hinged together. Three Euler angles about the hinge position defined the relative positions of the two YPK domains in question and a least-squares estimation of the Euler angles at each point of a grid of possible hinge locations was performed, which was similar to our refinement of the three QD coordinates. Whereas they employ molecular dynamics to estimate acceptor positions, we consider the acceptor positions as variables. We surveyed the possible acceptor locations, much as the YPK study surveyed their hinge position. The shorter linker between dye and cysteine sulfur atoms in the YPK system added legitimacy to the assumption of known acceptor positions. Additionally, the QD acts as both anchoring scaffold and energy donor as opposed to two dye labels being juxtaposed on different protein domains.

The final orientation suggests that MBP prefers a certain configuration relative to the QD. Although it appears that the MBP is free to rotate around the pentahistidine point of QD attachment, there is a preferred orientation and thus MBP does not ''flap'' around on its tether relative to the QD. Evidence for this possibility includes the small SD (range, 1–5%) of the FRET titrations and the relatively low Δ values when comparing the final calculated values with the measured values (range, 0–11%). We essentially arrived at one unique orientation, which is in agreement with our previous functional results. The refinement used had no weighting or constraints imposed on it, nor did the modeling constrain the orientation of the C-terminal pentahistidine sequence relative to the QD surface. This finding is important because the refined orientation produced this specific result without any input confirming that MBP coordinates to the QD surface by means of the C-terminal pentahistidine sequence (7). Specifically, Lys-370, adjoining the C-terminal Gly-Ser linker and pentahistidine sequence, is oriented closest to the QD surface. The MBP-binding site in this configuration is accessible to analytes, which is also in agreement with previous data (7). The refined distance from Lys-370 to the QD center is ≈45 Å, yielding an ≈90-Å diameter for the spheroid (Fig. 4). However, this value does not include the Gly-Ser linker and adjoining terminal pentahistidine sequence; see *Supporting Materials and Methods*. In a fully extended conformation, these seven residues would have an overall chain length of ≈25 Å (assuming a distance of 3.6 Å per residue and discounting the negligible contributions of side chains). The 555-nm QDs are expected to have a QD core–shell size of 60 Å (from the transmission electron microscopy and other data) and this diameter is expected to increase to 78–82 Å with the dihydrolipoic acid ligand cap (≈82 Å from the atomic force microscopy data) (24, 42, 46); see *Supporting Materials and Methods* and Figs. 5 and 6, which are published as supporting information on the PNAS web site. The difference between the QD spheroid diameter (≈90 Å) and the actual QD core–shell diameter (≈60 Å) is ≈30 Å, yielding an ≈15-Å distance from MBP Lys-370 to the QD ZnS shell surface. If all five histidines are coordinated to the QD surface, this distance should be ≈7 Å. The difference between 7 and 15 Å can be accounted for in several ways: a conservative estimate of ≈10–20% error in experimental measurements and subsequent refinement can be made; the MBP x-ray structure used is rigid, whereas the actual MBP-QD may alter conformation allosterically in response to C-terminal coordination (7); and the QDs used are not perfectly spherical in shape (although this is assumed), and this factor may also contribute experimental error.

The approach used here provides a generalized strategy for determining the orientation of a protein on a QD or other spherical nanoparticle. This approach will be applicable in cases where the orientation/conformation of a binding/active site of a protein relative to the nanoparticle is critical for recognition and function. This strategy is not limited to QDs, but may work with other nanoparticles that are either luminescent or function as dark quenchers. Furthermore, this process is not limited to QD–protein complexes alone, but may also function for the elucidation of the conformation of other labeled biomaterials attached to nanoparticle surfaces including DNA, polymers, dendrimers, peptides, and carbohydrates (as long as dyes can be site-specifically attached to them). This strategy may be particularly well suited for observing proteins that fold or change

conformation when attached to the surface of a QD (36, 37). For folding studies, the ability to control and predefine the molar ratio of specifically labeled protein to QD will be beneficial, because the increase in FRET acceptor cross section from multiple acceptor proteins arrayed around a single QD will increase sensitivity and allow even small conformational changes to be observed (7, 24). A potential limitation to this method involves overall protein and nanoparticle size, because neither participant can be so large as to preclude efficient FRET. This procedure may preclude its use in problems involving large red-emitting QDs ($\geq$ 10 nm), QD-nanorods with large aspect ratios, or large proteins such as antibodies. Additionally, some knowledge of the structure of both participants is required. In the case of proteins, crystallographic coordinates and the ability to make defined mutations and site specifically dye-label residues or regions will be necessary. Ultimately, this study provided a description of the MBP-QD nanoassembly and confirmed previous functional results (7, 24). Determining the structural properties of QD-bioreceptor assemblies will be important in developing QD-based reagentless sensors (39) and other bioconjugates employing luminescent nanocrystals or fluorescent/dark-quenching particles. It is well worth considering that even though a current focus of nanotechnology is in building the functional toolbox, mechanisms that model, predict, and monitor what exactly are being built are of equal importance.

We thank H. Hellinga (Duke University, Durham, NC) for the MBP plasmid. H.M. and J.M.M. thank K. Ward at the Office of Naval Research. This work was supported by Office of Naval Research Grant N001400WX20094. I.L.M. and A.R.C. are supported by a National Research Council Fellowship through the Naval Research Laboratory.

1. Niemeyer, C. M. (2001) *Angew. Chem. Int. Ed. Engl.* **40,** 4128–4158.
2. Willner, I. (2002) *Science* **298,** 2407–2408.
3. Emerich, D. F. & Thanos, C. G. (2003) *Expert Opin. Biol. Ther.* **3,** 655–663.
4. Sarikaya, M., Tamerler, C., Jen, A. K. Y., Schulten, K. & Baneyx, F. (2003) *Nat. Mater.* **2,** 577–585.
5. Behrens, S., Rahn, K., Habicht, W., Bohm, K. J., Rosner, H., Dinjus, E. & Unger, E. (2002) *Adv. Mater.* **14,** 1621–1625.
6. Mao, C. B., Flynn, C. E., Hayhurst, A., Sweeney, R., Qi, J. F., Georgiou, G., Iverson, B. & Belcher, A. M. (2003) *Proc. Natl. Acad. Sci. USA* **100,** 6946–6951.
7. Medintz, I. L., Clapp, A. R., Mattoussi, H., Goldman, E. R., Fisher, B. & Mauro, J. M. (2003) *Nat. Mater.* **2,** 630–638.
8. Paunesku, T., Rajh, T., Wiederrecht, G., Maser, J., Vogt, S., Stojicevic, N., Protic, M., Lai, B., Oryhon, J., Thurnauer, M. & Woloschak, G. (2003) *Nat. Mater.* **2,** 343–346.
9. Murphy, C. J. (2002) *Anal. Chem.* **74,** A520–A526.
10. Chan, W. C. W. & Nie, S. M. (1998) *Science* **281,** 2016–2018.
11. Bruchez, M., Moronne, M., Gin, P., Weis, S. & Alivisatos, A. P. (1998) *Science* **281,** 2013–2016.
12. Han, M. Y., Gao, X. H., Su, J. Z. & Nie, S. (2001) *Nat. Biotechnol.* **19,** 631–635.
13. Jaiswal, J. K., Mattoussi, H., Mauro, J. M. & Simon, S. M. (2003) *Nat. Biotechnol.* **21,** 47–51.
14. Goldman, E. R., Balighian, E. D., Mattoussi, H., Kuno, M. K., Mauro, J. M., Tran, P. T. & Anderson, G. P. (2002) *J. Am. Chem. Soc.* **124,** 6378–6382.
15. Goldman, E. R., Anderson, G. P., Tran, P. T., Mattoussi, H., Charles, P. T. & Mauro, J. M. (2002) *Anal. Chem.* **74,** 841–847.
16. Ishii, D., Kinbara, K., Ishida, Y., Ishii, N., Okochi, M., Yohda, M. & Aida, T. (2003) *Nature* **423,** 628–632.
17. Mattoussi, H., Mauro, J. M., Goldman, E. R., Anderson, G. P., Sundar, V. C., Mikulec, F. V. & Bawendi, M. G. (2000) *J. Am. Chem. Soc.* **122,** 12142–12150.
18. Akerman, M. E., Chan, W. C. W., Laakkonen, P., Bhatia, S. N. & Ruoslahti, E. (2002) *Proc. Natl. Acad. Sci. USA* **99,** 12617–12621.
19. Kloepfer, J. A., Mielke, R. E., Wong, M. S., Nealson, K. H., Stucky, G. & Nadeau, J. L. (2003) *Appl. Environ. Microbiol.* **69,** 4205–4213.
20. Wang, L. Y., Kan, X. W., Zhang, M. C., Zhu, C. Q. & Wang, L. (2002) *Analyst* **127,** 1531–1534.
21. Lin, Z. B., Cui, S. X., Zhang, H., Chen, Q. D., Yang, B., Su, X. G., Zhang, J. H. & Jin, Q. H. (2003) *Anal. Biochem.* **319,** 239–243.
22. Dahan, M., Levi, S., Luccardini, C., Rostaing, P., Riveau, B. & Triller, A. (2003) *Science* **302,** 442–445.
23. Patolsky, F., Gill, R., Weizmann, Y., Mokari, T., Banin, U. & Willner, I. (2003) *J. Am. Chem. Soc.* **125,** 13918–13919.
24. Clapp, A. R., Medintz, I. L., Mauro, J. M., Fisher, B., Bawendi, M. G. & Mattoussi, H. (2004) *J. Am. Chem. Soc.* **126,** 301–310.
25. Medintz, I. L., Trammell, S. A., Mattoussi, H. & Mauro, J. M. (2004) *J. Am. Chem. Soc.* **126,** 30–31.
26. Watrob, H. M., Pan, C.-P. & Barkley, M. D. (2003) *J. Am. Chem. Soc.* **125,** 7336–7343.
27. Krishnan, R. V., Varma, R. & Mayor, S. (2001) *J. Fluoresc.* **11,** 211–226.
28. Robinson, J. M., Dong, W.-J. & Cheung, H. C. (2003) *J. Mol. Biol.* **329,** 371–380.
29. Lafontaine, D. A., Norman, D. G. & Lilley, D. M. J. (2002) *EMBO J.* **21,** 2461–2471.
30. Vallotton, P., Tairi, A. P., Wohland, T., Friedrich-Benet, K., Pick, H., Hovius, R. & Vogel, H. (2001) *Biochemistry* **40,** 12237–12242.
31. Lin, R. C. & Scheller, R. H. (1997) *Neuron* **19,** 1087–1094.
32. Chen, X. H., Chu, M. H. & Giedroc, D. P. (1999) *Biochemistry* **38,** 12915–12925.
33. Damelin, M. & Silver, P. A. (2002) *Biophys. J.* **83,** 3626–3636.
34. Tung, C. S., Wall, M. E., Gallagher, S. C. & Trewhella, J. A. (2000) *Protein Sci.* **9,** 1312–1326.
35. Gaspar, R., Bagossi, P., Bene, L., Matko, J., Szollosi, J., Tozser, J., Fesus, L., Waldmann, T. A. & Damjanovich, S. (2001) *J. Immunol.* **166,** 5078–5086.
36. Lillo, M. P., Beechem, J. M., Szpikowska, B. K., Sherman, M. A. & Mas, M. T. (1997) *Biochemistry* **36,** 11261–11272.
37. Lillo, M. P., Szpikowska, B. K., Mas, M. T., Sutin, J. D. & Beechem, J. M. (1997) *Biochemistry* **36,** 11273–11281.
38. Medintz, I. L., Goldman, E. R., Lassman, M. E. & Mauro, J. M. (2003) *Bioconjugate Chem.* **14,** 909–918.
39. Marvin, J. S., Corcoran, E. E., Hattangadi, N. A., Zhang, J. V., Gere, S. A. & Hellinga, H. W. (1997) *Proc. Natl. Acad. Sci. USA* **94,** 4366–4371.
40. Sharff, A. J., Rodseth, L. E. & Quicho, F. A. (1993) *Biochemistry* **32,** 10553–10559.
41. Medintz, I. L & Mauro, J. M. (2004) *Anal. Lett.* **37,** 209–220.
42. Dabbousi, B. O., RodriguezViejo, J., Mikulec, F. V., Heine, J. R., Mattoussi, H., Ober, R., Jensen, K. F. & Bawendi, M. G. (1997) *J. Phys. Chem. B* **46,** 9463–9475.
43. Rubin, S. M., Lee, S. Y., Ruiz, E. J., Pines, A. & Wemmer, D. E. (2002) *Mol. Biol.* **322,** 425–440.
44. Ferrin, T. E., Huang, C. C., Jarvis, L. E. & Langridge, R. (1988) *J. Mol. Graphics.* **6,** 13–27.
45. Kasper, J. S. & Lonsdale, K., eds. (1972) in *International Tables for X-ray Crystallography* (Kynoch, Birmingham, U. K.), Vol. 2, pp. 330–331.
46. Parkinson, B.W. (1997) *J. Guidance Control Dyn.* **20,** 11–25.